Materials Today Chemistry 16 (2020) 100221

Contents lists available at ScienceDirect

Materials Today Chemistry

journal homepage: www.journals.elsevier.com/materials-today-chemistry/

Uncovering giant nanowheels for magnesium ion–based batteries

X. Fan [a], S. Garai [c], R.R. Gaddam [a], P.V. Menezes [d], D.P. Dubal [e], Y. Yamauchi [a], P.W. Menezes [b, *], A.K. Nanjundan [a, **], X.S. Zhao [a, ***]

[a] School of Chemical Engineering, The University of Queensland, St Lucia, Brisbane, 4072. Australia
[b] Department of Chemistry, Metalorganics and Inorganic Materials, Technische Universität Berlin, Strasse des 17. Juni 135, Sekr. C2, 10623 Berlin, Germany
[c] Department of Chemistry, National Institute of Technology, Tiruchirappalli, Tamil Nadu, 620015 India
[d] Institut für Elektrochemie, Universität Ulm, Albert-Einstein-Allee 47, D-89 081 Ulm, Germany
[e] School of Chemistry, Physics and Mechanical Engineering, Queensland University of Technology (QUT), 2 George Street, Brisbane, QLD, 4001, Australia

ARTICLE INFO

Article history:
Received 6 August 2019
Received in revised form
28 October 2019
Accepted 30 October 2019
Available online 20 January 2020

Keywords:
Giant nanowheels Mo_{154}
Magnesium-based batteries
Electron delocalization
Lattice water
Structure design
Hybrid Na–Mg ion battery

ABSTRACT

The giant wheel-shaped $Na_{15}\{[Mo_{154}O_{462}H_{14}(H_2O)_{70}]_{0.5}[Mo_{152}O_{457}H_{14}(H_2O)_{68}]_{0.5}\}\cdot$ca. 400 H_2O (Mo_{154}) is one of the fascinating clusters with the open host framework, which is designed by simple metal-oxygen fragment–linked coordination modes. The generation of structural vacancies (here referred to as defects), the substitution of ligands, and incorporation of heterometallic centers in Mo_{154} could offer several attractive possibilities to achieve good electrochemical performance such as high specific capacity and stability in multivalent batteries. Herein, we have introduced electronically rich giant nanowheel Mo_{154} as a potential cathode material in magnesium-rechargeable batteries (MRBs). The experimental evidence indicates that the Mo_{154} wheels offer a reversible capacity of ~150 mAh g^{-1} at 50 mA g^{-1} in MRBs, which was retained to about 55 mAh g^{-1} after a long cycling life (>500 cycles). Typically, the divalent alkali metals (Mg^{2+}) suffer from diffusion and insertion reactions in host materials; however, the stable and high rate performance against cycling with good Coulombic efficiency was achieved for Mo_{154} electrodes. Thus, the work demonstrates that the complex inorganic clusters are promising cathode materials in multivalent ion batteries.

1. Introduction

The next-generation energy storage devices based on multivalent metals such as magnesium (Mg) and calcium (Ca) metals as anode materials are acquiring increasing interest [1]not only because of their dendrite-free nature with improved safety and cycle life but also because of their multivalent nature, which can offer higher energy density (for Mg, gravimetric: 2205 mAh g^{-1}, volumetric: 3832 mAh cm^{-3}) than the lithium-ion batteries based on graphite anodes (~370 mAh g^{-1}) [2]. Moreover, magnesium-rechargeable batteries (MRBs) are very promising with intrinsic low reduction potential, small ionic radius, and highly reversible nature. It may also provide an opportunity for battery cost reductions because of its natural abundance in the earth's crust (5th most abundant element, approximately 24 times cheaper than Li) [1]. However, to explore the full potential of the MRBs, high-energy-density electrodes (especially cathode materials) need to be developed to guarantee high-energy output and structural stability to ensure long cycling performance. Recent studies have shown that the discovery of cathode materials is mainly inhibited by the nature of divalent Mg^{2+} ions: the high charge density (a double charge divided by a small radius of 0.74 Å) leads to reduced diffusivity within common polar crystalline hosts due to strong Coulombic interactions [3].

Despite the recent advancement in materials development for MRBs, including metal sulfides/selenides [1a,4], $MgMSiO_4$ (M = Fe, Mn, Co), [5], $MgFePO_4F$, [6], organic compounds, [7], Prussian blue , [8], the suitable cathode-host materials with fast charge kinetics is a bottleneck. So far, the most suitable cathode material with superior Mg^{2+} storage characteristics is still Chevrel phases (CPs) Mo_6S_8 reported in the pioneering work of Aurbach et al. [9] The unusual activity of CPs in the reversible processes of Mg^{2+} insertion/extraction can be attributed to the presence of octahedral Mo clusters in the crystal structure of these materials [10]. Because the

* Corresponding author.
** Corresponding author.
*** Corresponding author.
E-mail addresses: prashanth.menezes@mailbox.tu-berlin.de (P.W. Menezes), ashok.nanjundan@uq.edu.au (A.K. Nanjundan), george.zhao@uq.edu.au (X.S. Zhao).

https://doi.org/10.1016/j.mtchem.2019.100221
2468-5194/

crystal structure of CPs is composed of octahedral clusters of six Mo^{II} sites with metal-metal single bonds (the Mo_6T_8 blocks) face-capped by eight chalcogen ions, they can accommodate up to 4 electrons, thereby enhancing the kinetics of Mg^{2+} insertion [10]. In this regard, we have introduced another kind of material with Mo clusters as cathode materials for MRBs. The isolation of blue single crystals from the historical 'mysterious blue waters' enabled Müller and coworkers in 1995 to finally formulate Mo blue compound as a $\{Mo_{154}\} \equiv [Mo_{154}O_{448}(NO)_{14}H_{14}(H_2O)_{70}]^{28-}$ giant nanowheel [11]. In the past 20 years, several different wheel-shaped nanocontainer molecules were characterized by single-crystal X-ray structure determination and several other physical techniques, which broadly follow in two different classes: Mo_{154}, the big wheel and the Mo_{176}, the Bielefeld wheel [11]. Although the giant nanowheels and their derivatives have structurally been characterized, the potential of such remarkable clusters as functional materials has not been explored so far.

The Mo_{154} wheels are 'reduced protonated hydrated molybdenum oxides' as they can be expressed as $[(MoO_3)_{11n}H_n(H_2O)_{5n}]^{n-}$ where n = 14/16, and the presence of these 14 or 16 subunits can be monitored directly through scanning tunneling microscopic imaging and spectroscopic imaging [12]. The formulas can also be expressed in terms of their building blocks as $[\{Mo_8\}_n\{Mo_2\}_n\{Mo_1\}_n]^{n-}$. The $\{Mo_8\}$ core clusters with metal-metal chemical bonds, which can be regarded as a pseudo single-transition metal ion that can accommodate up to 28 electrons (compare to one or two electrons for a usual transition metal ion) [12]. Such cluster materials can be a promising host for multivalent ion because of the ability of redistribution of the bivalent cation charge of Mg^{2+} within the local crystal structure. This prompted us to investigate and introduce the role of Mo_{154} nanowheels as cathode material in magnesium ion and sodium-magnesium hybrid batteries. Based on the aforementioned considerations, we first report on giant nanowheel Mo_{154} as a potential cathode in MRBs. The Mo_{154} cathode delivered a reversible Mg^{2+} storage capacity of ~150 mAh g^{-1} at a current density of 50 mA g^{-1}, which was retained to about 55 mAh g^{-1} over a long cycling life (>500 cycles). A stable high rate cycle performance at 500 mA g^{-1} was also achieved with a Coulombic efficiency close to 100%. Owing to the unique structure of Mo_{154}, the issue in MRBs such as slow Mg^{2+} diffusion and complex bivalent charge redistribution were bypassed, which is investigated in detail using various materials characterizations and electrochemical analysis. Finally, we have proposed leveraging of Mo cluster compounds as host materials for a wide range of divalent metal ions, thereby opening new opportunities for next-generation energy storage applications.

2. Results and discussion

The Mo_{154} nanowheel was synthesized using a unique solution-based method (Supporting Information), yielding dark blue crystals. The unit cell parameters of these blue crystals are identical to the literature values. The polyhedral, ball and stick view of the Mo_{154} wheel is depicted in Scheme 1, displaying the original coordination geometry of the Mo-centers.

The experimental and simulated (from the crystal data) powder X-ray diffraction (PXRD) patterns (Debye type) of Mo_{154} (Supporting Information, Figure S1) reveals the close resemblance with large unit cell of Mo_{154}, which confers a large number of reflections with the separation less than the resolution of the diffractometer at the Cu-K_α wavelength, as well as by particle size broadening. The presence of a large number of lattice water molecules in the crystal structure of Mo_{154} leads to the reduction of crystallinity [13]. Scanning electron microscopy (SEM) and high-resolution (HR) SEM images demonstrate the agglomeration of large crystals (Supporting Information, Figure S2). Further, the Fourier transformed infrared (FT-IR) spectrum measured between 400 and 2000 cm^{-1} (Supporting Information, Figure S3) of Mo_{154} exhibited peaks at 1618 (m) (δ_{H2O}), 978 (m), 912 (w-m) ($\nu_{Mo]O}$), 810 (sh), 745 (s), 628 (s), 555 (s) ($\nu_{Mo\text{-}O\ and}\ \delta_{Mo\text{-}O}$) cm^{-1}. The electronic absorption (Supporting Information, Figure S4) spectrum shows two bands, which are characteristics for almost all molybdenum blue species. The intervalence (Mo^V –> Mo^{VI}) charge transfer (IVCT) transitions contribute to 5×10^3 per Mo^V sites in the visible/near-infrared [14] and thereby the lower energy transition reflects the presence of 28 electrons, which are inhomogeneously delocalized throughout the cluster skeleton showing a stronger preference for residence in the $\{Mo_8\}$ cores [12]. Furthermore, high-resolution transmission electron microscopy HR-TEM and selected area diffraction pattern studies (Supporting Information, Figure S5) were displayed large particles (supporting SEM analysis) but mostly of par reduced crystallinity becasue of higher weathering inside the microscope column. The presence of molybdenum was also additionally confirmed using energy-dispersive X-ray (EDX) analysis (Supporting Information, Figure S6). The electronic structure of the sample was examined by using X-ray photoelectron spectroscopy (XPS). The HR XPS scan of Mo 3d is shown in Fig. 1. The spin-orbit components of Mo $3d_{5/2}$ and Mo $3d_{3/2}$ can be fitted to well-resolved doublets. The major peaks at 233.3 and 236.4 eV could directly be ascribed to molybdenum (VI), whereas the minor peaks at 231.9 and 235.1 eV are correlated to molybdenum (V). The values and the corresponding oxidation states of Mo are well in agreement with the crystal structure of Mo_{154}, as well as to the previous MoO_x materials reported in the literature [15]. In the O 1s spectra, the peaks at 531.1, 532.2 eV, and 533.4 eV could be assigned to the μ_2/μ_3 −type O atoms, protonated O sites, and the water molecules of the crystal structure, respectively.

The electrochemical properties of Mo_{154} in traditional MRBs were studied in a potential window of 0.01–2.0 V *vs.* Mg^{2+}/Mg. Fig. 2a shows the galvanostatic charge/discharge curves of the Mo_{154} electrode at the current density of 50 mA g^{-1}. The cell exhibited sloping potential curves similar to that observed in electrochemical double-layer capacitors, and the initial discharge capacity was around 150 mAh g^{-1}. The absence of the reaction plateau indicates capacitive behavior. This can be attributed to the open structure and abundant defect sites of Mo_{154}, which highly enlarged the exposed active sites and enhanced the kinetics of charge transfer. The postmortem HR-TEM analysis shown in Figure S7 suggests the amorphous nature of Mo_{154} without obvious fringes. After fully charging and discharging, the Mo_{154} still shows an amorphous network with numerous vacancies. The XPS HR spectra of Mg 2p of cycled Mo_{154} further confirm the successful storage of Mg^{2+} ions (Figure S8).

The cycling stability of Mo_{154} electrode is shown in Fig. 2c. The cell retained a reversible capacity of around 55 mAh g^{-1} after 500 cycles at 50 mA g^{-1}. The obvious capacity decay during the first few cycles was observed, suggesting inaccessibility of some electrochemical active sites of Mo_{154}; however, the performance is still very promising compared with other Mo-based materials with different structures and compositions as tabulated in Table S1. Further, the rate performance of Mo_{154} is also encouraging as shown in Fig. 2b. The capacity obtained at high current rates was recovered when the current density switched back to low, indicating good structural stability of Mo_{154} at high current density. The high capacity retention over long-term cycling reflects the good stability of Mo_{154}. The long-term stability of Mo_{154} in Magnesium ion batteries (MIBs) was further recorded by cycling the battery at 500 mA g^{-1} for 500 cycles (Fig. 2c). The Mo_{154} electrode maintained a discharge capacity of ~30 mAh g^{-1} after 500 cycles. The Coulombic efficiency was maintained at 100%, which can be

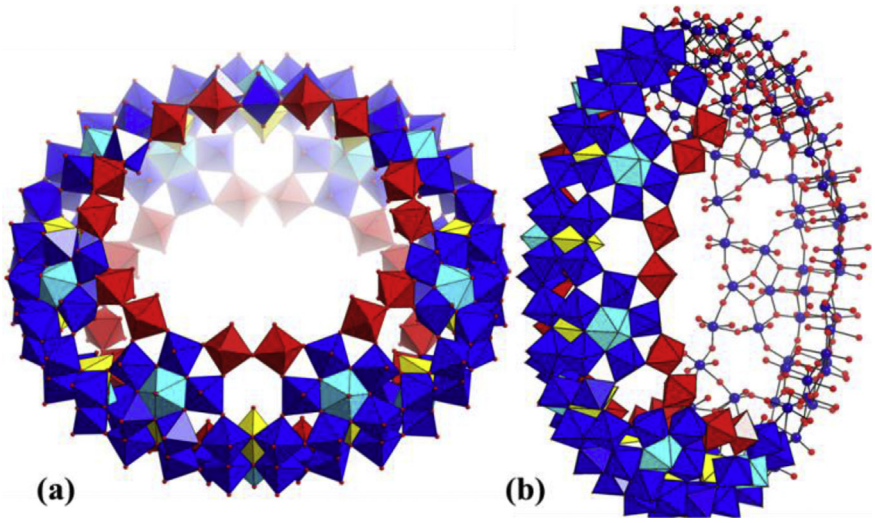

Scheme 1. Polyhedral (a) and ball and stick (b) representation of Mo_{154} nanocapsule exhibiting different subunits [$Mo_{154} \equiv (Mo_8)_{14}(Mo_2)_{14}(Mo_1)_{14}$] in various color. The {Mo_8} units are colored in blue, whereas the {Mo_2} and {Mo_1} units are represented in red and yellow, respectively. The central pentagonal bipyramidal coordination of Mo-centers is epitomized in light blue whereas approximate octahedrally coordinated Mo sites are in dark blue.

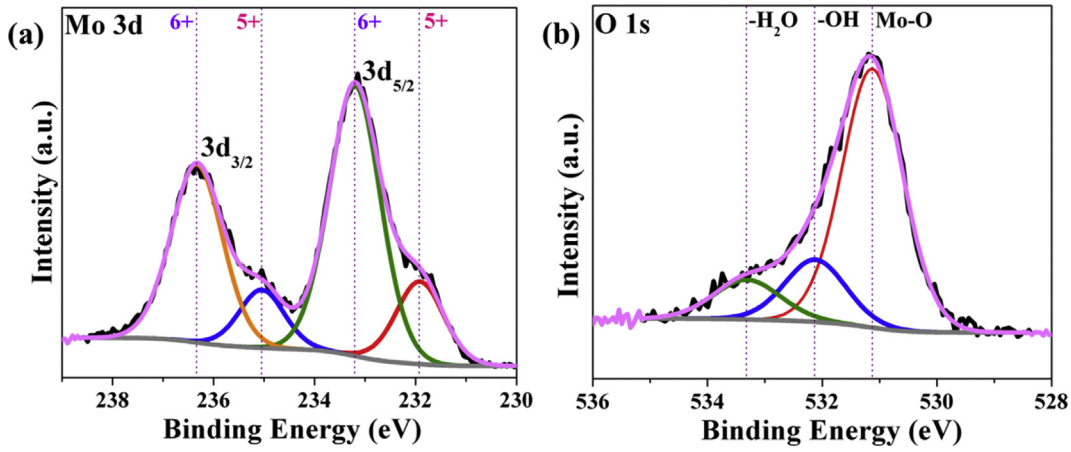

Fig. 1. The deconvoluted XPS high-resolution spectra of (a) Mo 3d and (b) O 1s. XPS, x-ray photoelectron spectroscopy.

attributed to negligible charge trapping at the cathode in subsequent cycles, as well as the highly reversible and dendrite-free nature of the Mg anode. Therefore, the present work shows that the Mo_{154} with the open framework crystal structure can efficiently host divalent insertion cations at high rates to produce unprecedented cycle life and coulombic efficiencies.

An alternative battery concept that takes full advantage of the metallic Mg anode but bypasses the need for an efficient Mg cathode material is the hybrid Mg-Li/Na battery. This hybrid design could integrate the advantages of the Mg metal anode and the Li^+/Na^+ storage cathode for providing a device with much better cycle performance, which has been investigated in several recent proof-of-concept reports [1]. Particularly, the Mg-Na hybrid battery (MNIB) system has a potential advantage to fully exploit the cost benefits when compared with Mg-Li hybrid system by simply shifting from Li-containing electrolyte and Li cathode chemistry to Na-based alternatives. With this motivation, we have investigated the performance of Mo_{154} in MNIBs, as shown in Fig. 3. The 0.2 M [Mg_2Cl_2][$AlCl_4$]$_2$/DME electrolyte, was chosen as the MNIB electrolyte. The capacity of the MNIB system can reach ~250 mAh g^{-1} during the first three cycles at a current density of 50 mA g^{-1}. As shown in the charge-discharge curves, it can be observed that charge capacity is larger than that of the discharge capacity, which can be attributed to the existed delocalized Na^+ ions associated with the giant wheel-shaped clusters $Na_{15}\{[Mo_{154}O_{462}H_{14}(H_2O)_{70}]_{0.5}$ $[Mo_{152}O_{457}H_{14}(H_2O)_{68}]_{0.5}\}\cdot ca.400$ H_2O that gradually released during cycling. The Na^+ ions are removed from the host structures with the reversible partial concomitant oxidation of the Mo clusters [16]. This does not happen in the MRBs, where no extra capacity contribution was observed during the charging process, indicating that Mg^{2+} insertion or storage does not involve the release of Na^+, as well as the oxidation of Mo. This can be confirmed in the cyclic voltammetry (CV) curve of MRB and MNIB shown in Fig. 4, where no peaks are shown in MRB CV curve, indicating a capacitance behavior. Whereas, the CV curve of MNIB shows a large anodic peak around 1.2 V in the first scan, which disappeared in the following cycles, confirming the extra Na^+ extraction from the Mo_{154} in the first charging process. The Na^+ ions, which lie in the ion migration pathway, can be removed or exchanged with Mg^{2+} to allow better

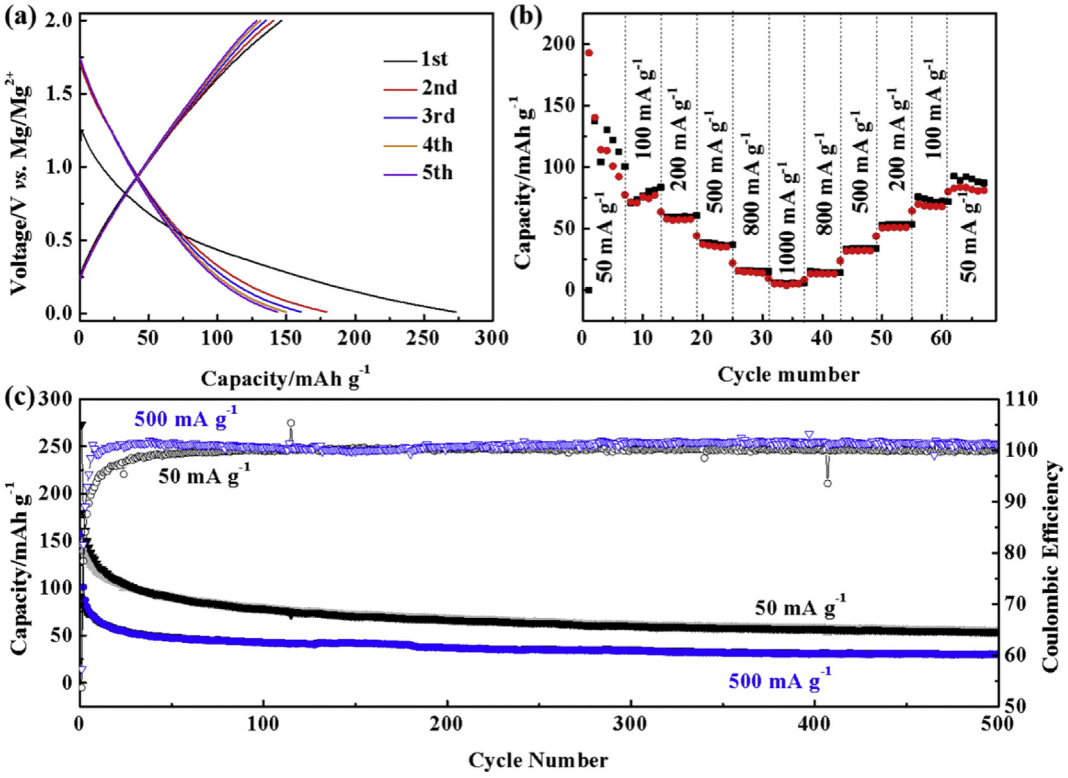

Fig. 2. (a) First five charge-discharge profiles of Mo_{154} at 50 mA g^{-1} in MRBs. (b) Rate performance of Mo_{154} at various current densities in MRBs. (c) Cycle stability of Mo_{154} at 50 mA g^{-1} and 500 mA g^{-1} of Mo_{154} as cathodes for MRBs. MRBs, magnesium-rechargeable batteries.

Mg^{2+} extraction. Despite the improved capacities, the poor cycle stability of MNIB is still a bottleneck, which needs further investigations.

Besides the large electrostatic interaction between insertion ions and host anions, the difficulty in redistributing the divalent charge of Mg^{2+} to achieve local electroneutrality leads to slow kinetics and poor cycle ability [10,17]. For most of the commonly studied intercalation compounds, it is difficult to undergo electrochemical processes with a charge transfer of more than one electron per ion. Besides, the abrupt change in the oxidation state of transition metal cations upon multielectron redox processes should result in the drastic local deformations in the crystal structure of the host [18]. Here we have compared the performance of Mo_{154} with other Mo-based materials that applied in MRBs. As summarized in supporting information Table S1, Mo_{154} showed a capacity of ~110 mAh g^{-1} at 50 mA g^{-1} after 20 cycles and ~91 mA g^{-1} after 50 cycles, which are higher than most of the reported materials. After 500 cycles, it still delivered comparable capacity retention at similar current density, indicating good stability among the reported results [9,19]. The charge storage mechanism has not been fully elucidated, however, based on the previous attributions several hypotheses may help to explain the enhanced performance of Mo_{154}, some of them are as follows:

(1) Mo_{154} clusters belong to the 'Robin-Day classification III' because of the complete delocalization of the two 4d electrons in the $\{Mo_5O_6\}$ compartment. This electron delocalization, which is responsible for the intense blue color of these clusters, exhibits two intervalence charge transfer bands at the wavelength of 750 nm and 1050 nm. Quantitative characterization is also possible *via* the extinction coefficient of the higher wavelength band ($\varepsilon = 5000$ $mol^{-1}dm^3cm^{-1}/Mo^V$ centers) [14]. Because a giant wheel-shaped clusters Mo_{154} comprise 14 incomplete cubane-type $\{Mo_5O_6\}$ compartments, each containing two delocalized 4d electrons, the Mo_{154} cluster has 28 delocalized 4d electrons. Upon insertion of one Mg^{2+} ion per formula unit, the formal charge of the individual Mo ion in the cluster changes only by 1 of 14 electron. This is a great advantage to help redistribute the divalent charge to achieve local electroneutrality. As a result, the Mo_{154} clusters may not only enable the fast and reversible storage of Mg^{2+} but also be favorable for various cations, including monovalent (Li^+, Na^+, Cu^+), as well as other divalent cations (Zn^{2+}, Ca^{2+}, Cd^{2+}, Ni^{2+}, Mn^{2+}, Co^{2+}, Fe^{2+}) at ambient temperatures.

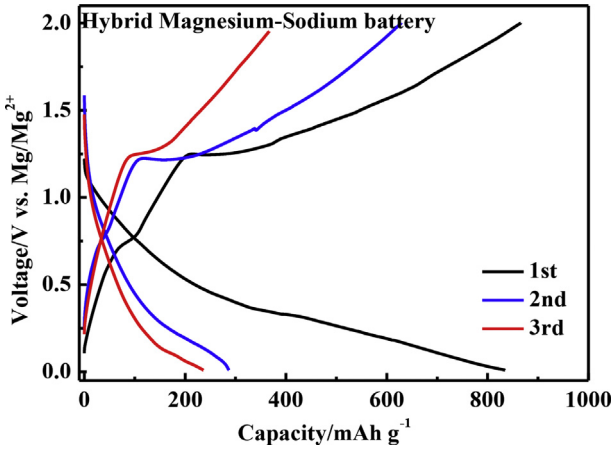

Fig. 3. Voltage curves of the Mo_{154} applied as cathode material for Mg-Na hybrid battery at 50 mA g^{-1}.

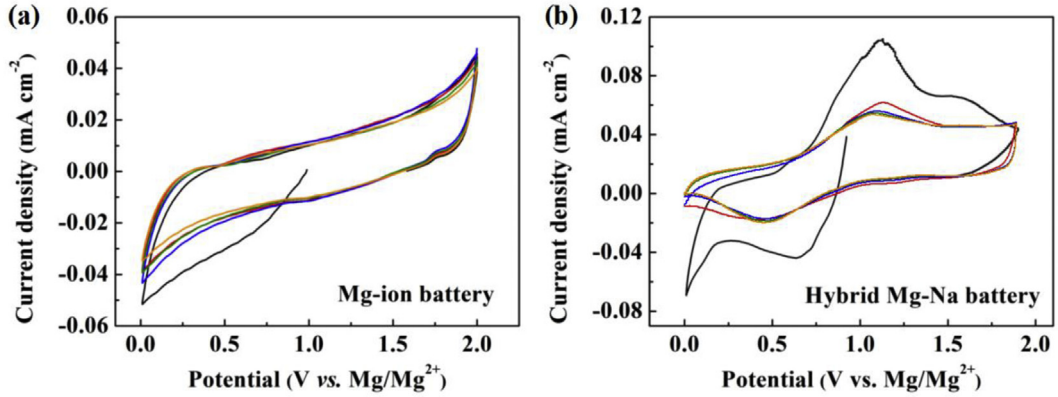

Fig. 4. Cyclic voltammograms of Mo_{154} in (a) MRBs and (b) MNIB at a scan rate of 0.2 mV s^{-1}. MNIB, Mg-Na hybrid battery; MRBs, magnesium-rechargeable batteries.

(2) The addition of Na^+ can further promote the performance of Mo_{154} in Mg^{2+} storage, where the exchanged Na^+ can form diffusion channels for Mg^{2+} transport, despite the fast capacity decay.
(3) The Mo_{154}-type wheels having an average external diameter of 3.4 nm and height 1.5 nm (small ionic radii, Mg^{2+}: 0.72 Å) [20] are not compact. This exposed flatness of the Mo_{154}-type wheel might increase the accessibility of its surface toward the ions in the electrolyte and contribute to rapid ionic diffusion [21]. Moreover, the labile corner-shared $[Mo_2O_5(H_2O)_2]^{2+}$ may also be reversibly replaced, as known for several nicked structures, [14], and therefore, it can produce additional sites for the placement of Mg^{2+} ions.
(4) the crystal $[(MoO_3)_{11n}H_n(H_2O)_{5n}]^{n-}$ (n = 14/16) contains a large number of lattice water molecules, [12], which can transform Mg^{2+} into much less polarizing solvated ions, thereby alleviating the host-guest interaction and increasing the ion diffusivity [19b].
(5) The origination of hydrophilic surface is consistent with the option for the {H_2O—Mo=O} functional groups to exist in another orientation such as {O=Mo—OH_2}, which triggers the polymerization of the lower charges wheels *via* the formation of Mo—O—Mo linkages resulting 2D chain or layer structures in specific cases [14]. Furthermore, this type of fast tumbling of protons may constitute its basis for the very high alkali/alkaline earth metal conductivity.

3. Conclusion

In conclusion, we have investigated the Mg^{2+} storage properties of giant nanowheels-shaped $Na_{15}\{[Mo_{154}O_{462}H_{14}(H_2O)_{70}]_{0.5}[Mo_{152}O_{457}H_{14}(H_2O)_{68}]_{0.5}\}\cdot$ca. 400 H_2O (Mo_{154}) clusters. The Mo_{154} wheels exhibited a reversible Mg^{2+} storage capacity of ~150 mAh g^{-1} at a current density of 50 mA g^{-1} in MRBs and retained of about 55 mAh g^{-1} after a long cycling life (>500 cycles). The stable high-rate cycle performance at 500 mA g^{-1} with a coulombic efficiency close to 100% can be attributed to the unique crystal structure and electrical properties of the materials. These features described vide supra make Mo_{154} uniquely suited for multivalent ion storage, thus opening up broad-ranging applications beyond multivalent ion storage, such as ion sensing, ion separation, and wastewater treatment. However, further investigation, such as synchrotron X-ray diffraction and extended X-ray absorption fine structure is required to fully understand the roles of lattice water molecules, crystal vacancies, and the easy divalent charge redistributing in assisting the insertion process in Mo_{154} local structure.

4. Experimental section

4.1. Chemicals

All chemical reagents (analytical grade) were used as received without any further purification. Deionized water was used throughout the experiment.

4.2. Characterization

PXRD patterns were obtained on a Bruker AXS D8 advanced automatic diffractometer equipped with a position-sensitive detector and curved germanium (111) primary monochromator using Cu Kα radiation (λ = 1.5418 Å). FT-IR spectra were recorded on a Thermofisher Nicolet iS5 IR spectrometer (ATR-Diamond). Ultraviolet-visible (UV-vis) spectra were monitored on an Analytik Jena Specord S600 spectrophotometer and the WinAspect 2.3.1.0 software package using a 1 cm quartz cell at room temperature. Inductively coupled plasma atomic emission spectroscopy was carried out in a Thermo Jarrell Ash Trace Scan analyzer. The samples were digested in aqua regia, and the average of three reproducible independent experiments has been presented. SEM was carried out on an LEO DSM 982 microscope integrated with EDX (EDAX, Apollo XPP). Data handling and analyses were achieved with the software package EDAX. TEM was accomplished on an FEI Tecnai G2 20 S-TWIN transmission electron microscope (FEI Company, Eindhoven, Netherlands) equipped with a LaB6 source at 200 kV acceleration voltage. EDX analyses were achieved with an EDAX r-TEM SUTW detector (Si [Li] detector), and the images were recorded with a GATAN MS794 P CCD camera. The SEM and TEM experiments were conducted at the Zentrum für Elektronenmikroskopie of the TU Berlin. XPS spectra were acquired on a Kratos Axis ULTRA X-ray photoelectron spectrometer. The binding energies were calibrated relative to the C 1s peak energy position as 285.0 eV. Data analyses were carried out using Casa XPS.

4.3. Synthesis of $Na_{15}\{[Mo_{154}O_{462}H_{14}(H_2O)_{70}]_{0.5}[Mo_{152}O_{457}H_{14}(H_2O)_{68}]_{0.5}\}\cdot$ca. 400 H_2O (Mo_{154})

To a stirred solution of $Na_2MoO_4\cdot 2H_2O$ (3.0 g, 12.4 mmol) in 10 mL of water, powdered $Na_2S_2O_4$ (0.2 g, 1.15 mmol) was added which imparted a light-yellow coloration to the solution. 30 mL of hydrochloric acid (1 M, standardized) was then added to the mixture at once which immediately changed the solution color to deep blue. The stirring of the solution was continued for an additional 15 min to ensure the generation of enough reduced Mo sites to continue the process of self-assembly. Thereafter, the solution

was stored undisturbed in a closed flask at 20 °C (optimal). After one week, the precipitated blue crystals were removed by filtration, washed very quickly (extremely soluble) with a small amount of cold water to remove the excess NaCl and dried at room temperature over dry $CaCl_2$. Yield: 0.7 g (28% based on Mo).

4.4. Single-crystal X-ray unit cell determination

Several crystals were mounted and measured using Siemens AXS SMART system (three-circle diffractometer with CCD-detector), Mo-K_α radiation ($\lambda = 0.71073$ Å), graphite monochromator, crystal size 0.2 x 0.2 × 0.08 mm3, 183 K. The observed unit cell was triclinic, space group P-1, $a = 24.834(5)$ Å, $b = 35.753(4)$ Å, $c = 44.598(3)$ Å, $\alpha = 93.22(2)$ °, $\beta = 93.49(4)$°, $\gamma = 106.71(1)$°, $V = 37635(3)$ Å^3 which are in very good agreement with the reported values [22]. The structural graphics was performed using with DIAMOND 2.1 from K. Brandenburg, Crystal Impact GbR, 2001.

4.5. Preparation of electrolyte

The electrolyte synthesis was carried out inside an argon filled glovebox. An all-phenyl complex (APC) electrolyte was used in fabricating the MRB cell and synthesized in a glove box filled with high purity argon gas. 0.25 M AlCl3 (Sigma Aldrich, 563919) in anhydrous tetrahydrofuran (THF) (Sigma Aldrich, 186562) solution was slowly added dropwise to 2 M phenyl magnesium chloride solution in THF (Sigma Aldrich, 224448) under vigorous stirring to form the APC electrolyte of 0.25 M concentration. As for Mg-Na dual ion battery, in a typical synthesis of 0.2 M $[Mg_2Cl_2][AlCl_4]_2$/DME electrolyte, 0.267 g $AlCl_3$ powder (Sigma Aldrich, 563919) was added slowly (exothermic reaction) to a suspension of 0.19 g $MgCl_2$ (Alfa Aesar, 42850) in 5-ml DME in a 10-ml glass vial. The mixture was stirred at 60 °C using a sand bath for 6 h and was cooled to room temperature. A clear solution was obtained with no precipitants. The hybrid-ion electrolyte was prepared by dissolving an appropriate amount of $NaAlCl_4$ (Sigma Aldrich, 451584) into the aforementioned electrolyte.

4.6. Preparation of electrode

The Mo_{154} electrodes were fabricated by mixing 80% Mo154, 10% polyvinylidene fluoride and 10% carbon black. The average active loading of Mo154 on each electrode is ~0.8 mg. The components were ground together with a mortar and pestle in a small amount of 1-methyl-2-pyrrolidinone to form slurry that was then deposited onto a carbon cloth current collector. These electrodes were dried under vacuum at 80 °C and assembled into 2032-type coin cells with magnesium ribbon (Sigma Aldrich, 13103) as the anode and Celgard 3501 as the separator. The Mg ribbon was polished using sandpaper to remove the oxide layer.

Conflict of competing interest

The authors declare no conflict of interest.

Acknowledgements

This work was partly supported by the University of Queensland's UQ Fellowship and a UQ Early Career Researcher Grant (UQECR1719813). The authors also gratefully acknowledge the facilities and technical assistance of the Australian Microscopy and Microanalysis Research Facility at the UQ Centre for Microscopy and Microanalysis. This work was performed in part at the Queensland node of the Australian National Fabrication Facility Queensland Node (ANFF-Q), a company established under the National Collaborative Research Infrastructure Strategy to provide nano- and micro-fabrication facilities for Australia's researchers.

Appendix A. Supplementary data

Supplementary data to this article can be found online at https://doi.org/10.1016/j.mtchem.2019.100221.

References

[1] a) Y. Gu, Y. Katsura, T. Yoshino, H. Takagi, K. Taniguchi, Rechargeable magnesium-ion battery based on a $TiSe_2$-cathode with d-p orbital hybridized electronic structure, Sci. Rep. 5 (2015) 12486;
b) J.-H. Cho, M. Aykol, S. Kim, J.-H. Ha, C. Wolverton, K.Y. Chung, K.-B. Kim, B.-W. Cho, Controlling the intercalation chemistry to design high-performance dual-salt hybrid rechargeable batteries, J. Am. Chem. Soc. 136 (2014) 16116–16119;
c) R.C. Massé, E. Uchaker, G. Cao, Beyond Li-ion: electrode materials for sodium- and magnesium-ion batteries, Sci. China Mater. 58 (2015) 715–766.

[2] D. Aurbach, Y. Gofer, Z. Lu, A. Schechter, O. Chusid, H. Gizbar, Y. Cohen, V. Ashkenazi, M. Moshkovich, R. Turgeman, E. Levi, A short review on the comparison between Li battery systems and rechargeable magnesium battery technology, J. Power Sources 97–98 (2001) 28–32.

[3] a) M.E. Spahr, P. Novák, O. Haas, R. Nesper, Electrochemical insertion of lithium, sodium, and magnesium in molybdenum(VI) oxide, J. Power Sources 54 (1995) 346–351;
b) P.G. Bruce, F. Krok, J. Nowinski, V.C. Gibson, K. Tavakkoli, Chemical intercalation of magnesium into solid hosts, J. Mater. Chem. 1 (1991) 705–706;
c) D. Aurbach, I. Weissman, Y. Gofer, E. Levi, Nonaqueous magnesium electrochemistry and its application in secondary batteries, Chem. Rec. 3 (2003) 61–73;
d) R.C. Massé, E. Uchaker, G. Cao, Beyond Li-ion: electrode materials for sodium- and magnesium-ion batteries, Sci. China Mater. 58 (2015) 715–766.

[4] a) X. Fan, R.R. Gaddam, N.A. Kumar, X.S. Zhao, A hybrid Mg^{2+}/Li^+ battery based on interlayer-expanded MoS_2/graphene cathode, Adv. Energy Mater. 7 (2017) 1700317;
b) B. Liu, T. Luo, G. Mu, X. Wang, D. Chen, G. Shen, Rechargeable Mg-ion batteries based on WSe_2 nanowire cathodes, ACS Nano 7 (2013) 8051–8058;
c) S.C. Singh, H. Li, C. Yao, Z. Zhan, W. Yu, Z. Yu, C. Guo, Structural and compositional control in copper selenide nanocrystals for light-induced self-repairable electrodes, Nano Energy 51 (2018) 774–785.

[5] a) Y. Orikasa, T. Masese, Y. Koyama, T. Mori, M. Hattori, K. Yamamoto, T. Okado, Z.-D. Huang, T. Minato, C. Tassel, J. Kim, Y. Kobayashi, T. Abe, H. Kageyama, Y. Uchimoto, High energy density rechargeable magnesium battery using earth-abundant and non-toxic elements, Sci. Rep. 4 (2014) 5622;
b) Y. NuLi, J. Yang, Y. Li, J. Wang, Mesoporous magnesium manganese silicate as cathode materials for rechargeable magnesium batteries, Chem. Commun. 46 (2010) 3794–3796;
c) Y. Zheng, Y. NuLi, Q. Chen, Y. Wang, J. Yang, J. Wang, Magnesium cobalt silicate materials for reversible magnesium ion storage, Electrochim. Acta 66 (2012) 75–81.

[6] Z.-D. Huang, T. Masese, Y. Orikasa, T. Mori, T. Minato, C. Tassel, Y. Kobayashi, H. Kageyamac, Y. Uchimotoa, $MgFePO_4F$ as a feasible cathode material for magnesium batteries, J. Mater. Chem. A 2 (2014) 11578–11582.

[7] a) H. Sano, H. Senoh, M. Yao, H. Sakabe, T. Kibayashi, Mg^{2+} storage in organic positive-electrode active material based on 2,5-Dimethoxyl-1,4-benzoquinone, Chem. Lett. 41 (2012) 1594–1596;
b) R. Zhang, F. Mizuno, C. Ling, Fullerenes: non-transition metal clusters as rechargerable magnesium battery cathodes, Chem. Commun. 51 (2015) 1108–1111.

[8] R.Y. Wang, C.D. Wessells, R.A. Huggins, Y. Cui, Highly reversible open framework nanoscale electrodes for divalent ion batteries, Nano Lett. 13 (2013) 5748–5752.

[9] D. Aurbach, Z. Lu, A. Schechter, Y. Gofer, H. Gizbar, R. Turgeman, Y. Cohen, M. Moshkovich, E. Levi, Prototype systems for rechargeable magnesium batteries, Nature 407 (2000) 724–727.

[10] E. Levi, M.D. Levi, O. Chasid, D. Aurbach, A review on the problems of the solid state ions diffusion in cathodes for rechargeable Mg batteries, J. Electroceram. 22 (2007) 13–19.

[11] A. Müller, S.Q.N. Shah, H. Bögge, M. Schmidtmann, Molecular growth from a Mo_{176} to a Mo_{248} cluster, Nature 397 (1999) 48–50.

[12] D. Zhong, F.L. Sousa, A. Müller, L. Chi, H. Fuchs, A nanosized molybdenum oxide wheel with a unique electronic-necklace structure: STM study with submolecular resolution, Angew. Chem. Int. Ed. 50 (2011) 7018–7021.

[13] S. Garai, E.T.K. Haupt, H. Bögge, A. Merca, A. Müller, Picking up 30 CO_2 molecules by a porous metal oxide capsule based on the same number of receptors, Angew. Chem. Int. Ed. 51 (2012) 10528–10531.

[14] A. Muller, P. Gouzerh, From linking of metal-oxide building blocks in a dynamic library to giant clusters with unique properties and towards adaptive chemistry, Chem. Soc. Rev. 41 (2012) 7431–7463.

[15] J.G. Choi, L.T. Thompson, XPS study of as-prepared and reduced molybdenum oxides, Appl. Surf. Sci. 93 (1996) 143–149.
[16] H. Yaghoobnejad Asl, P. Stanley, K. Ghosh, A. Choudhury, Iron borophosphate as a potential cathode for lithium-and sodium-ion batteries, Chem. Mater. 27 (2015) 7058–7069.
[17] G.G. Amatucci, F. Badway, A. Singhal, B. Beaudoin, G. Skandan, T. Bowmer, I. Plitz, N. Pereira, T. Chapman, R. Jaworski, Investigation of yttrium and polyvalent ion intercalation into nanocrystalline vanadium oxide, J. Electrochem. Soc. 148 (2001) A940–A950.
[18] P. Novák, W. Scheifele, O. Haas, Magnesium insertion batteries-an alternative to lithium? J. Power Sources 54 (1995) 479–482.
[19] a) Q.D. Truong, M. Kempaiah Devaraju, D.N. Nguyen, Y. Gambe, K. Nayuki, Y. Sasaki, P.D. Tran, I. Honma, Disulfide-bridged (Mo_3S_{11}) cluster polymer: molecular dynamics and application as electrode material for a rechargeable magnesium battery, Nano Lett. 16 (2016) 5829–5835;
b) Y. Liang, H.D. Yoo, Y. Li, J. Shuai, H.A. Calderon, F.C. Robles Hernandez, L.C. Grabow, Y. Yao, Interlayer-expanded molybdenum disulfide nanocomposites for electrochemical magnesium storage, Nano Lett. 15 (2015) 2194–2202;
c) Y. Liang, R. Feng, S. Yang, H. Ma, J. Liang, J. Chen, Rechargeable Mg batteries with graphene-like MoS_2 cathode and ultrasmall Mg nanoparticle anode, Adv. Mater. 23 (2011) 640–643;
d) Y. Liu, L. Jiao, Q. Wu, J. Du, Y. Zhao, Y. Si, Y. Wang, H. Yuan, Sandwich-structured graphene-like MoS_2/C microspheres for rechargeable Mg batteries, J. Mater. Chem. A 1 (2013) 5822–5826.
[20] H.D. Yoo, I. Shterenberg, Y. Gofer, G. Gershinsky, N. Pour, D. Aurbach, Mg rechargeable batteries: an on-going challenge, Energy Environ. Sci. 6 (2013) 2265–2279.
[21] A. Müller, C. Serain, Soluble Molybdenum Blues-“des Pudels Kern”, Acc. Chem. Res. 33 (2000) 2–10.
[22] A. Müller, S.K. Das, V.P. Fedin, E. Krickemeyer, C. Beugholt, H. Bögge, M. Schmidtmann, B. Hauptfleisch, Rapid and simple isolation of the crystalline molybdenum-blue compounds with discrete and linked nanosized ring-shaped anions: $Na_{15}[Mo_{126}Mo_{28}O_{462}H_{14}(H_2O)_{70}]_{0.5}$ $[Mo_{124}Mo_{28}O_{457}H_{14}(H_2O)_{68}]_{0.5}\cdot$ ca. $400H_2O$ and $Na_{22}[Mo_{118}Mo_{28}O_{442}H_{14}(H_2O)_{58}]\cdot$ ca. $250H_2O$, Z. Anorg. Allg. Chem. 625 (1999) 1187–1192.